Landslides, earthquakes, and erosion

Bruce D. Malamud[a],[*], Donald L. Turcotte[b], Fausto Guzzetti[c], Paola Reichenbach[c]

[a]*Environmental Monitoring and Modeling Research Group, Department of Geography, King's College London, Strand, London, WC2R 2LS, United Kingdom*
[b]*Department of Geology, University of California, Davis, CA 95616, USA*
[c]*IRPI CNR, via della Madonna Alta 126, Perugia 06128, Italy*

Abstract

This paper relates landslide inventories to erosion rates and provides quantitative estimates of the landslide hazard associated with earthquakes. We do this by utilizing a three-parameter inverse-gamma distribution, which fits the frequency–area statistics of three substantially 'complete' landslide-event inventories. A consequence of this general distribution is that a landslide-event magnitude $m_L=\log N_{LT}$ can be introduced, where N_{LT} is the total number of landslides associated with the landslide event. Using this general distribution, landslide-event magnitudes m_L can be obtained from incomplete landslide inventories, and the total area and volume of associated landslides, as well as the area and volume of the maximum landslides, can be directly related to the landslide-event magnitude. Using estimated recurrence intervals for three landslide events and the time span for two historical inventories, we estimate regional erosion rates associated with landslides as typically 0.1–2.5 mm year^{-1}. We next give an empirical correlation between the earthquake magnitude, associated landslide-event magnitude, and the total volume of associated landslides. Using these correlations, we estimate that the minimum earthquake magnitudes that will generate landslides is $M=4.3\pm0.4$. Finally, using Gutenberg–Richter frequency-magnitude statistics for regional seismicity, we relate the intensity of seismicity in an area and the magnitude of the largest regional earthquakes to erosion rates. We find that typical seismically induced erosion rates in active subduction zones are 0.2–7 mm year^{-1} and adjacent to plate boundary strike-slip fault zones are 0.01–0.7 mm year^{-1}.
© 2004 Elsevier B.V. All rights reserved.

Keywords: landslides; earthquakes; erosion; hazard assessment; mathematical modeling

1. Introduction

Landslide events are generally associated with a trigger such as an earthquake, a large storm, a rapid snowmelt, or a volcanic eruption. A landslide event may include a single landslide or many thousands and

---

* Corresponding author. Tel.: +44 0207 848 2466.
E-mail addresses: bruce@malamud.com (B.D. Malamud), turcotte@geology.ucdavis.edu (D.L. Turcotte), fausto.guzzetti@irpi.cnr.it (F. Guzzetti), paola.reichenbach@irpi.cnr.it (P. Reichenbach).

can be quantified by the frequency–area distribution of the triggered landslides. We have recently shown [1] that the frequency–area statistics of three substantially complete landslide inventories are well approximated by the same probability density function, a three-parameter inverse-gamma distribution. We also introduced a landslide-event magnitude scale $m_L=\log(N_{LT})$, with N_{LT} the total number of landslides associated with the landslide event, in analogy to the Richter earthquake magnitude scale. In this paper, we use this general landslide distribution to (a) relate landslide inventories to erosion rates and (b) provide quantitative estimates of the landslide hazard associated with earthquakes.

In Section 2 of this paper, we use the general landslide probability distribution to relate the total area, number, and volume of landslides associated with a landslide event to the landslide-event magnitude. This distribution can also be used to obtain a landslide-event magnitude for incomplete event inventories, as long as the inventory is complete for the largest landslides [1]. In Section 3, we examine historical landslide inventories, the sum of landslide events over time. One consequence of the general landslide distribution is that a historical inventory will have the same distribution of landslide areas as a single landslide event. In Section 4, we utilize the concept of a general landslide distribution to improve our understanding of the landslide hazard associated with earthquakes. Earthquakes are a major cause of landslides, which, in turn, are a major cause of the damage and casualties associated with earthquakes [2–5]. To quantify this association, we combine our landslide distribution with an empirical relationship proposed by Keefer [4] relating the total volume of landslides generated by an earthquake and the earthquake's moment magnitude. We then relate the earthquake moment magnitude to the total number of associated landslides and landslide-event magnitude, and compare our predictions with data compilations given by Keefer [5]. Finally, in Section 5, we consider rates of erosion associated with landslides. We estimate erosion rates associated with three substantially complete landslide-event inventories and two historical inventories. We then use the Gutenberg–Richter frequency–magnitude relation for earthquakes to obtain an analytic expression for erosion rates in terms of the frequency of occurrence

of earthquakes. Variables used in the text, along with their decription, are given in Appendix A.

2. Quantifying landslide events

2.1. Landslide probability distribution

To give the statistical distribution of landslide areas, a probability density function $p(A_L)$ is defined according to

$$p(A_L) = \frac{1}{N_{LT}} \frac{\delta N_L}{\delta A_L} \tag{1}$$

with the normalization condition

$$\int_0^\infty p(A_L) \mathrm{d}A_L = 1 \tag{2}$$

where A_L is landslide area, N_{LT} is the total number of landslides in the inventory, and δN_L is the number of landslides with areas between A_L and $A_L + \delta A_L$. In Fig. 1, we present the probability densities $p(A_L)$ for three substantially complete landslide inventories: (i) N_{LT}=11,111 landslides triggered by the magnitude M=6.7 Northridge earthquake (California, USA) on 17 January 1994 [6,7]; (ii) N_{LT}=4223 landslides in the Umbria region (Italy), triggered by rapid snowmelt in January 1997 [8,9]; and (iii) N_{LT}=9594 landslides in Guatemala, triggered by heavy rainfall from Hurricane Mitch in late October and early November 1998 [10]. A detailed discussion of each inventory is found in [1].

The three sets of probability densities given in Fig. 1 exhibit a characteristic shape [1,9], with densities increasing to a maximum value (most abundant landslide size) and then decreasing with a power-law tail. The inventories were estimated [6–10] to be nearly complete for landslides with length scales greater than 5–15 m ($A_L \approx 25$–225 m^2), therefore, the 'rollover' in Fig. 1 is regarded as real. Based on the good agreement between these three sets of probability densities, we proposed [1] a general probability distribution for landslides, a three-parameter inverse-gamma distribution, given by [11,12]

$$p(A_L; \rho, a, s) = \frac{1}{a\Gamma(\rho)} \left[\frac{a}{A_L - s} \right]^{\rho+1} \exp\left[-\frac{a}{A_L - s} \right] \tag{3}$$
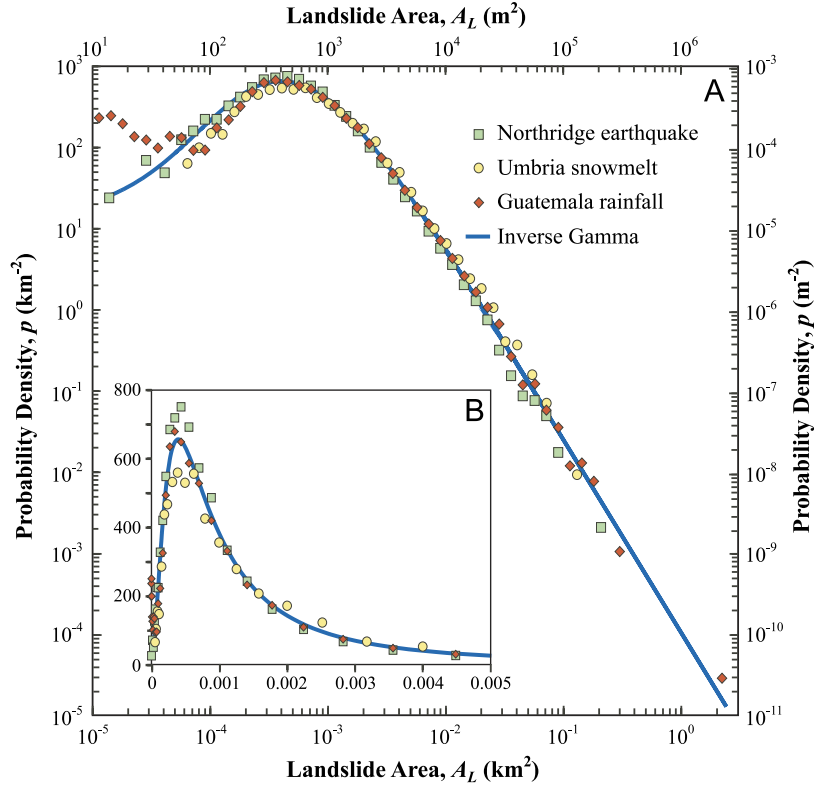
Fig. 1. Dependence of the landslide probability densities p on landslide area A_L for three landslide inventories: (1) 11,111 landslides triggered by the 17 January 1994 Northridge earthquake in California [6,7]; (2) 4233 landslides triggered by rapid snowmelt in the Umbria region of Italy in January 1997 [8,9]; (3) 9594 landslides triggered by heavy rainfall from Hurricane Mitch in Guatemala in late October and early November 1998 [10]. Probability densities are given on logarithmic axes in Panel A and linear axes in Panel B. Also included is our proposed general landslide probability distribution. This is the best fit to the three landslide inventories of the three-parameter inverse-gamma distribution (Eq. (3)), with $\rho=1.40$, $a=1.28\times10^{-3}$ km^2, and $s=-1.32\times10^{-4}$ km^2 (coefficient of determination $r^2=0.965$). Figure after [1], reproduced with permission, John Wiley and Sons Limited.

where $\Gamma(\rho)$ is the gamma function of ρ. The inverse-gamma distribution has a power-law decay with exponent $-(\rho+1)$ for medium and large areas and an exponential rollover for small areas. The maximum likelihood fit of Eq. (3) to the data sets in Fig. 1 yields $\rho=1.40$, $a=1.28\times10^{-3}$ km^2, and $s=-1.32\times10^{-4}$ km^2, with a coefficient of determination $r^2=0.965$; the power-law tail has an exponent $\rho+1=2.40$. Many authors (see [1] for a review) have also noted that the frequency–area distribution of large landslides correlate with a power-law tail. This common behaviour is observed despite large differences in landslide types, topography, soil types, and triggering mechanisms.

On the basis of the good agreement between the three landslide inventories and the inverse-gamma distribution illustrated in Fig. 1, we hypothesized [1] that the distribution given in Eq. (3) is general for landslide events. It is not expected that all landslide-event inventories will be in as good agreement as the three considered, but we do argue that the quantification, if only approximate, is valuable in assessing the landslide hazard.

2.2. Landslide areas and volumes

Using the general landslide distribution given in Eq. (3), equations were derived [1] quantifying the

average, total, and maximum landslide areas and volumes associated with a landslide event. The required integrations are dominated by the power-law tail of the medium and large landslides vs. the much smaller contribution of the exponential rollover for small landslides (see Eq. (3)). In the integrations, the largest landslides play a larger role for volumes than for area. The results obtained were [1] the following:

Average landslide area:

$$\bar{A}_{\mathrm{L}}[\mathrm{km}^2] = \int_0^\infty A_{\mathrm{L}} p(A_{\mathrm{L}}) \mathrm{d}A_{\mathrm{L}} = \frac{a}{\rho - 1} + s$$
$$= 3.07 \times 10^{-3} \qquad (4)$$

Average landslide volume:

$$\bar{V}_{\mathrm{L}}[\mathrm{km}^3] = (7.30 \times 10^{-6}) N_{\mathrm{LT}}^{0.122} \qquad (5)$$

Total landslide area:

$$A_{\mathrm{LT}}[\mathrm{km}^2] = \bar{A}_{\mathrm{L}} N_{\mathrm{LT}} = (3.07 \times 10^{-3}) N_{\mathrm{LT}} \qquad (6)$$

Total landslide volume:

$$V_{\mathrm{LT}}[\mathrm{km}^3] = N_{\mathrm{L}} \bar{V}_{\mathrm{LT}} = (7.30 \times 10^{-6}) N_{\mathrm{LT}}^{1.122} \qquad (7)$$

Maximum landslide area:

$$A_{\mathrm{Lmax}}[\mathrm{km}^2] = (1.10 \times 10^{-3}) N_{\mathrm{LT}}^{0.714} \qquad (8)$$

Maximum landslide volume:

$$V_{\mathrm{Lmax}}[\mathrm{km}^3] = (1.82 \times 10^{-6} \ \mathrm{km}^3) N_{\mathrm{LT}}^{1.071} \qquad (9)$$

In Eqs. (4)–(9), N_{LT} is the total number of landslides in a 'complete' inventory of a landslide event. The mean area $\bar{A}_{\mathrm{L}}$ is independent of N_{LT}, but the mean volume $\bar{V}_{\mathrm{L}}$ increases with N_{LT}. Conversions from area to volume were based on an empirical scaling relationship from Hovius et al. [13]:

$$V_{\mathrm{L}} = \varepsilon A_{\mathrm{L}}^{1.50} \qquad (10)$$

with $\varepsilon = 0.05 \pm 0.02$ (see [1] for discussion).

2.3. Landslide magnitude scale

We also proposed [1] a magnitude scale m_{L} for a landslide event based on the logarithm to the base 10

of the total number of landslides associated with the landslide event:

$$m_{\mathrm{L}} = \log N_{\mathrm{LT}} \qquad (11)$$

Keefer [3] and later Rodríguez et al. [14] used a similar scale to quantify the number of landslides in earthquake-triggered landslide events: 100–1000 landslides were classified as a two, 1000–10,000 landslides a three, etc. The total measured area A_{LT} and volume V_{LT} of landslides associated with a landslide event can also be used to determine the landslide magnitude m_{L}. Assuming the applicability of our general landslide distribution, we combine Eqs. (6) and (7) with Eq. (11) to give

$$m_{\mathrm{L}} = \log A_{\mathrm{LT}} + 2.51 = 0.89 \log V_{\mathrm{LT}} + 4.58 \qquad (12)$$

with A_{LT} in km^2 and V_{LT} in km^3. We will now apply the ideas of a general landslide distribution for events to historical landslide inventories.

3. Historical landslide inventories

Historical landslide inventories include the sum of many landslide events that have occurred over time. Assuming that our landslide probability distribution is applicable to all landslide events, the sum of events over time (the historical inventory) will also satisfy this distribution [1]. However, in historical inventories, the evidence for the existence of many smaller and medium landslides will have been lost due to wasting processes over time. Therefore, for the historical inventories, we attribute the deviation from our general landslide distribution to the incompleteness of the inventories. Using the general landslide distribution (Eq. (3)) we can extrapolate an inventory that contains just the largest landslides to give the total number and total volume of all landslides in the region.

We will illustrate this extrapolation by considering two examples. We use frequency densities here since the inventories are incomplete and the normalization

given in Eq. (2) no longer holds. From Eq. (1), we note that the frequency density is

$$f(A_L) = \frac{\delta N_L}{\delta A_L} = N_{LT} p(A_L) \qquad (13)$$

Theoretical curves of $f(A_L)$ for various landslide-event magnitudes m_L are obtained by multiplying the probability distribution $p(A_L)$ given in Eq. (3) by the total number of landslides in the event N_{LT}. Curves are given in Fig. 2 for $m_L=1$ ($N_{LT}=10$) to $m_L=8$ ($N_{LT}=10^8$).

Included in Fig. 2 are the frequency densities for two historical landslide inventories from Italy and

Japan. Also included in Fig. 2, for reference, are frequency densities for the snowmelt-triggered Umbria landslide event (Fig. 1). The first historical inventory includes 44,724 landslides in the Umbria area of Italy [15] estimated to have occurred in the last 5–10 ky (thousand years). The power-law tail of the frequency densities is in good agreement with the landslide-event probability distribution (Eq. (3)). With a landslide magnitude $m_L=5.8\pm0.1$, we estimate that, over the last 5–10 ky, the total number of landslides that have occurred is $N_{LT}=650,000\pm150,000$. Substituting this value into Eq. (7), we find that the total volume of these landslides is $V_{LT}=24.3\pm6.3$ km^3. The second historical inventory
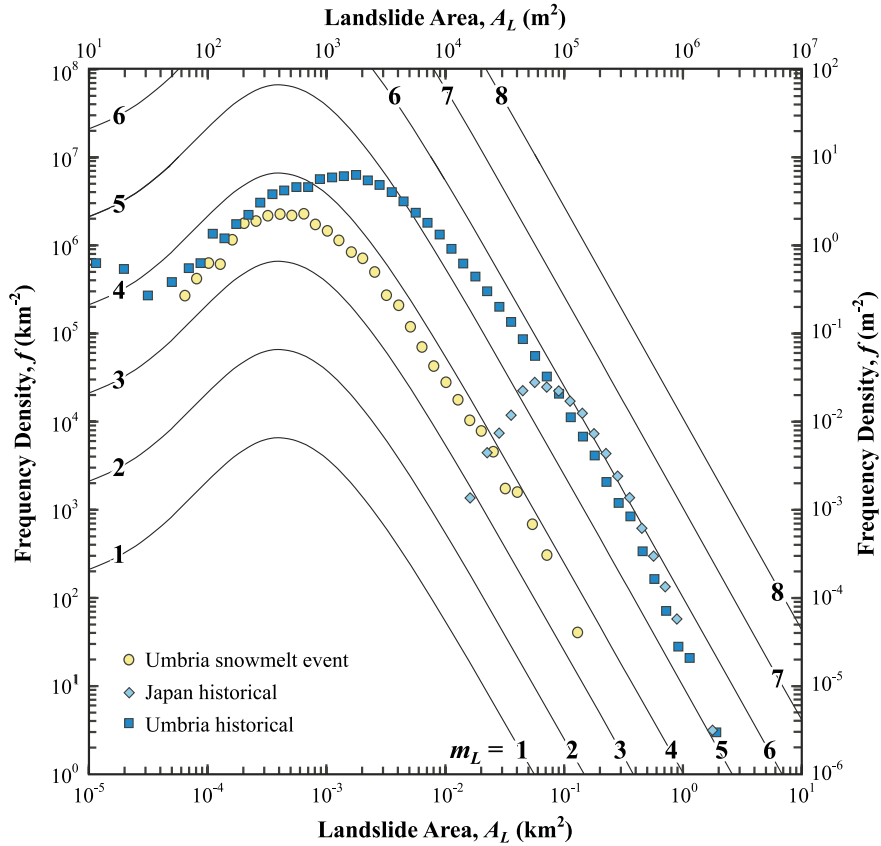

Fig. 2. Dependence of the landslide frequency density f on landslide area A_L, both on logarithmic axes. Landslide frequency distributions corresponding to our proposed landslide probability distribution (Eqs. (3) and (18)) are given for landslide magnitudes $m_L=1, 2, \ldots, 8$ ($N_{LT}=10$, $10^2, \ldots, 10^8$). Also included are the frequency densities for three landslide inventories: (1) Umbria snowmelt-triggered landslides as in Fig. 1; (2) 3424 historical landslides in the Akaishi Ranges of central Japan [16] estimated to have occurred in the last 10 ky; (3) 44,724 historical landslides in the Umbria region of Italy [15] estimated to have occurred in the last 5–10 ky.

in Fig. 2 includes 3424 landslides in the Akaishi Ranges of central Japan [16] estimated to have occurred in the last 10 ky. The power-law tail of the frequency densities gives m_L=6.0±0.2, corresponding to N_{LT}=1,100,000±500,000 and (Eq. (7)) V_{LT}=44.0±22.3 km^3. In Section 5, we will use these results to quantify regional erosion rates. However, before doing this, we examine the relationship of earthquakes to landslides.

4. Correlations between earthquake magnitude and landslide-event magnitude

Keefer [4] obtained an empirical correlation between the total volume of landslides triggered by an earthquake V_{LT} and the earthquake's moment magnitude M. He considered the total volume of landslide material generated by 15 historical earthquakes, as determined by several investigators using aerial photographs and field investigations. Despite the wide variety of geo-

logical (topography and rock type), geophysical (earthquake type and depth), and climatic conditions associated with these earthquake-triggered landslide events, a reasonably good power-law dependence of the total landslide volume V_{LT} on the earthquake's moment magnitude M was established. The data used by Keefer [4,5] are given in Fig. 3 and Table 1, along with the total landslide volume obtained for the 1994 Northridge earthquake (M=6.7) calculated by converting each landslide area to a volume using Eq. (10) and summing. The least-square best-fit line to the log V_{LT} vs. M data gives

$$\log V_{LT} = 1.42M - 11.26(\pm 0.52) \tag{14}$$

with V_{LT} in km^3. The error bounds (±0.52) represent the standard deviations of the fit. This correlation (solid line), along with the error bounds (dashed-lines), are given in Fig. 3. The correlation given in Eq. (14) differs slightly from that of Keefer [4] due to the addition of the Northridge data point.

Combining Eqs. (12) and (14), we relate the magnitude of the landslide event m_L to the earthquake moment magnitude M and obtain the result

$$m_L = 1.27M - 5.45(\pm 0.46) = \log N_{LT} \tag{15}$$

This dependence is given in Fig. 4, along with the corresponding error bounds. Included in Fig. 4 and Table 1 are the observational landslide-event magnitudes m_L and the corresponding number of landslides N_{LT} for 11 earthquakes as given by Keefer [5]. The theory curves in Fig. 4 have been derived from our empirical fit to the volumes in Fig. 3 using Eq. (3). We consider the agreement of the data given in Fig. 4 with the theoretical prediction very good, considering the wide range of seismic and geomorphic conditions under which earthquake-induced landslides occur.

The onset of landslides associated with earthquakes can be obtained by setting m_L=0 (N_{LT}=1, i.e., just one earthquake-triggered landslide) in Eq. (15), giving a threshold moment magnitude M= 4.3±0.4. This theoretical result corresponds with general observations made by Keefer [3] and Bommer and Rodríguez [17], who discuss the local and surface-wave magnitude of small earthquakes asso-
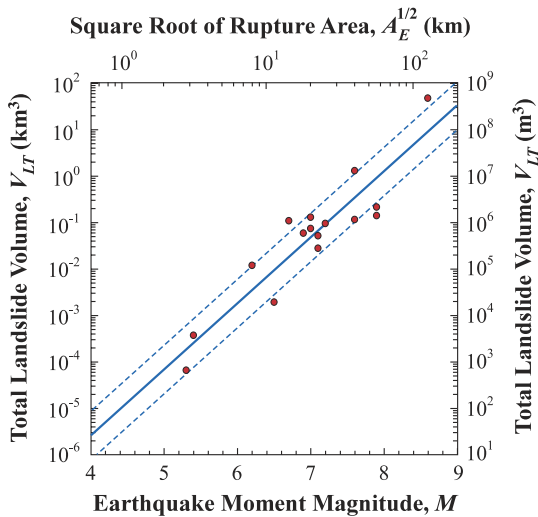

Fig. 3. The total volume of landslides V_{LT} triggered by an earthquake is given as a function of the earthquake moment magnitude M. Also given is the square root of the equivalent rupture area $A_E^{1/2}$. Circles are volumes of landslides associated with 16 landslide events, as given in Table 1. The solid line is the least-square best-fit straight line to the data (Eq. (14)); dashed lines give the standard deviations of the data with respect to the best fit.

Table 1
Earthquake location, date and moment magnitude M, along with corresponding volume V_{LT} and number of landslides N_{LT} associated with the earthquake (after Keefer[a] [4,5])

Location	Date	M	V_{LT} (km^3)	N_{LT}
Arthur's Pass, New Zealand	9 Mar 1929	6.9	5.90×10^{-02}	
Buller, New Zealand	17 Jun 1929	7.6	1.30×10^{0}	
Torricelli Mtns., New Guinea	20 Sep 1935	7.9	2.15×10^{-01}	
Assam, India	15 Aug 1950	8.6	$4.70 \times 10^{+01}$	
Daily City, CA, USA	22 Mar 1957	5.3[b]	6.70×10^{-05}	23
Inangahua, New Zealand	23 May 1968	7.1	5.20×10^{-02}	
Peru	31 May 1970	7.9	1.41×10^{-01}	
Papua New Guinea	31 Oct 1970	7.1	2.80×10^{-02}	
Guatemala	4 Feb 1976	7.6	1.16×10^{-01}	50,000
Darien, Panama	11 Jul 1976	7.0	1.30×10^{-01}	
Mt. Diablo, CA, USA	24 Jan 1980	5.8[b]		103
Mammoth Lakes, CA, USA	25 May 1980	6.2	1.20×10^{-02}	5253
Coalinga, CA, USA	2 May 1983	6.5	1.94×10^{-03}	9389
San Salvador, El Salvador	10 Oct 1986	5.4	3.78×10^{-04}	216
Ecuador	5 Mar 1987	7.2	9.53×10^{-02}	
Loma Prieta, CA, USA	17 Oct 1989	7.0	7.45×10^{-02}	1500
Northridge, CA, USA	17 Jan 1994	6.7	1.20×10^{-01} [c]	11,000
Hygoken-Nanbu, Japan	17 Jan 1995	6.9		700
Umbria-Marche, Italy	26 Sep 1997	6.0		110
Chi-Chi, Taiwan	21 Sep 1999	7.7		22,000

[a] Except as noted for Northridge, earthquake location, date, and moment magnitude M, along with estimated volume V_{LT} and number N_{LT} of landslides associated with the earthquake, are from extensive compilations of other studies by Keefer ([4], table 1; [5], table 2).

[b] Earthquake magnitudes are all moment or equivalent moment magnitudes except for Mt. Diablo (surface-wave magnitude) and Daily City (local magnitude) [4,5].

[c] The volume of landslides triggered by the 1994 Northridge earthquake was calculated by converting each inventory landslide area to a volume using Eq. (10) and summing.

ciated with landsliding. In general, for small earthquakes (magnitudes <5.5), the local (M_L), body-wave (m_b), surface-wave (M_s), and moment magnitudes (M) give approximately equivalent results [18]. Keefer [3] studied intensity reports and associated landslides from several hundred mostly small earthquakes in the United States (1958–1977). He suggests that the threshold below which landslides are not triggered by an earthquake has a local magnitude $M_L \approx 4.0$. Rodríguez et al. [14] have also considered this problem, with 36 worldwide earthquakes, and suggest higher values. Bommer and Rodríguez [17] have considered 62 Central American earthquakes during the period 1898–2001, each of which generated landslides. The smallest of these earthquakes that generated landslides had a surface wave magnitude $M_s \approx 4.8$. These results are consistent with our theoretical extrapolation.

We next relate the earthquake moment magnitude M to the total landslide area A_{LT} (Eqs. (12) and (15)), area of the largest triggered landslide A_{Lmax} (Eqs. (8) and (15)), and the volume of the largest triggered landslide V_{Lmax} (Eqs. (9) and (15)) and obtain

$$\log A_{LT} \left[\text{km}^2 \right] = 1.27M - 7.96(\pm 0.46) \qquad (16)$$

$$\log A_{Lmax} \left[\text{km}^2 \right] = 0.91M - 6.85(\pm 0.33) \qquad (17)$$

$$\log V_{Lmax} \left[\text{km}^3 \right] = 1.36M - 11.58(\pm 0.49) \qquad (18)$$

These are given in Fig. 5, along with the corresponding error bounds. As an example of the use of these relationships (Eqs. (14)–(18); Fig. 5), we consider an $M=8$ earthquake and find (with the range based on each equation's error bounds) the following:

We suggest that these values are reasonable upper and lower bounds for landslides triggered by a 'great' earthquake ($M=8$) in southern California.

Description	Variable	Value	Range	Unit
Landslide-event magnitude	m_L	4.71	(4.25–5.17)	
Number of associated landslides	N_{LT}	51,000	(18,000–148,000)	number
Total area of associated landslides	A_{LT}	158	(55–457)	km^2
Total volume of associated landslides	V_{LT}	1.26	(0.38–4.17)	km^3
Area of maximum landslide	A_{Lmax}	2.69	(1.26–5.75)	km^2
Volume of maximum landslide	V_{Lmax}	0.20	(0.06–0.62)	km^3

It should be emphasized that the magnitude of an earthquake-generated landslide event m_L is not simply a function of earthquake moment magnitude M. Other factors related to the earthquake include depth of rupture, direction of energy focusing, and regional attenuation. These are in addition to geomorphic considerations, such as roughness of topography, rock types, and hydrological conditions. However, we believe that even approximate correlations can provide important limits on the landslide hazard associated with earthquakes and associated rates of erosion.

An interesting question is whether these results might be of use in paleoseismicity studies. An estimate of the area or volume of a very old landslide believed to have been seismically triggered can be made, taking into account appropriate degradation of the landslide over time, and then the results given above used to arrive at a lower-bound moment magnitude for the earthquake that triggered the landslide. It is then possible, using radiocarbon and other dating techniques, to date these large landslides. An excellent review of studies and discussion of the use of landslides for paleoseismic analysis has been given by Jibson [19]. It would be an interesting test to see if any large landslide in southern California coincides with the dates of great earthquakes on the San Andreas Fault, obtained using standard paleoseismic techniques. Then, the area or volume of the landslide would provide a lower-bound estimate of the earthquake moment magnitude.

5. Erosion rates

5.1. Introduction

Burbank [20] has provided an extensive review of rates of erosion. He discusses how combinations of geobarometers and geochronometers give erosion rates in the range $\dot{h}=1$–30 mm year^{-1}, whereas weathering rates are typically in the range 0.005–0.02 mm year^{-1}. Thus, weathering rates are incapable of producing the rapid unloading indicated by the pressure–temperature–time studies. Burbank [20] argues that the dominant mechanism contributing to long-term erosion rates are glacial erosion, bedrock landslides, and massive rock falls. For the western flank of the Southern Alps, New Zealand, Hovius et al. [13] estimated a mean erosion rate caused by landslides of 9 ± 4 mm year^{-1}. In this section, we quantify erosion based on (a) event and historical landslide inventories, (b) earthquake-triggered landslides, (c) aftershocks, and (d) seismicity on a global scale.
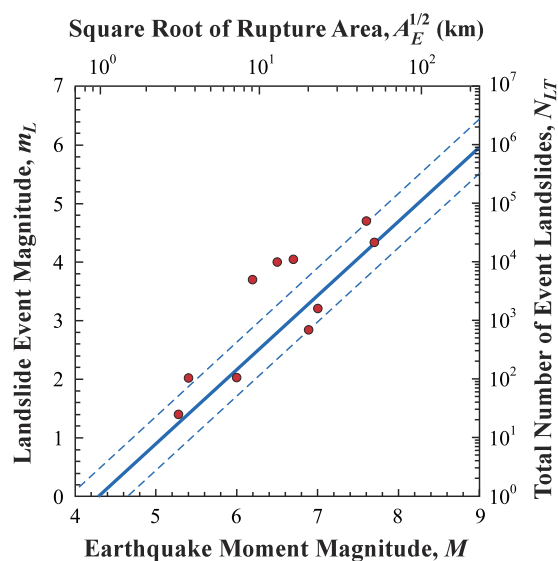

Fig. 4. Dependence of landslide-event magnitude m_L and total number of landslides N_{LT} on earthquake moment magnitude M. Also given is the square root of the equivalent rupture area $A_E^{1/2}$. The solid line is the correlation from Eq. (15), and the dashed lines are the corresponding error bounds. Also given are observational data for 11 earthquakes as given in Table 1.
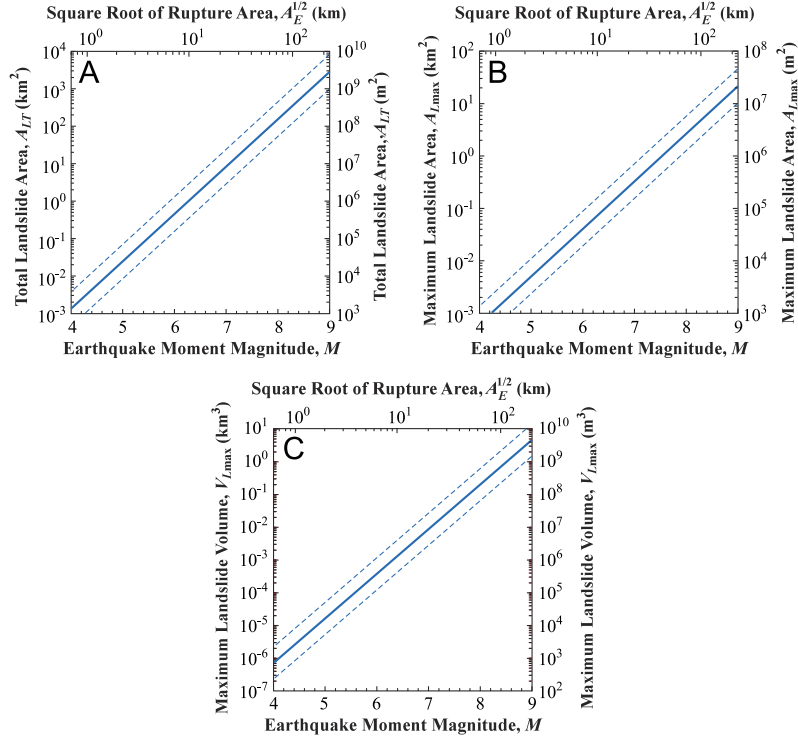
Fig. 5. Dependence on earthquake moment magnitude M of the (A) total area of landslides A_{LT}, (B) maximum landslide area A_{Lmax}, and (C) volume of the maximum landslide V_{Lmax}. Also given is the square root of the equivalent rupture area $A_E^{1/2}$. The solid lines are the correlations from (A) Eq. (16), (B) Eq. (17), and (C) Eq. (18). The dashed lines are the error bounds given in each equation.

5.2. Erosion based on event and historical landslide inventories

We use our quantifications of event and historical landslide inventories to estimate erosion rates. For the event inventories, we assume that there is a characteristic-sized trigger (e.g., largest earthquake) for the region that is repeated at regular intervals τ_L with the same total landslide volume V_{LT}. For historical landslide inventories, the 'repeat time' τ_L is the time interval over which the historical landslides accumulated. We define A_R as the area over which landslides are concentrated and assume that erosion in this area is dominated by these landslides. Although some material generated by landslides finds its way directly into the fluvial system, there is a residence time for other material that is temporarily stored in hill slopes. This includes material that may stay in approximately the same location and be 'reactivated' in subsequent landslides. For the purpose of our calculations, we will neglect this residence time, thus, our estimates will be

upper bounds for erosion in each case. With these assumptions, the erosion rate $\dot{h}$ is given by

$$\dot{h} = \frac{V_{LT}}{A_R \tau_L} \tag{19}$$

We use Eq. (19) to provide rough estimates of erosion rates associated with our three landslide-event inventories and two historical inventories, using the parameter values given in Table 2. We stress that the input values (and resultant erosion rates) are all rough estimates. The inferred regional erosion rates due to landslides for the Northridge earthquake-triggered, Umbria snowmelt-triggered, and Guatemala rainfall-triggered landslide events are 0.1, 0.3, and 2.5 mm year^{-1}, respectively. In comparison, the inferred long-term erosion rates due to landslides in Italy and Japan, the two historical inventories, are 0.4 and 2.2 mm year^{-1}, respectively. For the Umbria (Italy) area, the two inferred erosion rates are very similar (0.3 vs. 0.4 mm year^{-1}), despite one erosion rate being based on an individual event

Table 2
Estimates of regional erosion $\dot{h}$ based on landslide inventories

Landslide inventory	V_{LT}[a] (km^3)	A_R[b] (km^2)	τ_L[c] (years)	$\dot{h}$[d] (mm year^{-1})
Northridge earthquake-triggered event	0.1	1000	1000	0.1
Umbria snowmelt-triggered event, central Italy	0.7	2000	100	0.3
Guatemala rainfall-triggered event	0.5	2000	100	2.5
Umbria historical inventory, central Italy	24.	8000	8000	0.4
Akaishi ranges, Central Japan historical inventory	44.	2000	10,000	2.2

  [a] The total volume V_{LT} of associated landslides. This was calculated for the three event inventories by converting each inventory landslide area to a volume using Eq. (10) and summing, and for the two historical inventories by using the method as described in Section 3.

  [b] The area A_R over which landslides are concentrated. For each inventory, the locations of the landslides were examined spatially, and a rough estimate was made of the area A_R over which a high percentage of inventory landslides are concentrated. In most inventories, the landslides were found to be concentrated in those areas with medium to significant relief. Note that A_R is not necessarily as large as the area over which the inventory was originally compiled.

  [c] Recurrence interval, τ_L. For the three event inventories, beginning with the size of the trigger that resulted in the specific event, we estimate the average time between triggers with the same size or larger. For the two historical inventories, the 'recurrence interval' is taken to be the time interval over which the historical landslides accumulated.

  [d] Erosion rate $\dot{h}$ calculated using Eq. (19). Note that this does not take into account residence time of landslides in the system.

and the other on the sum of many events over thousands of years. For the four countries considered, the event and historical landslide inventories give regional erosion rates $h \approx 0.1$–2.5 mm year^{-1}. Considering the uncertainties in our parameter values and the variations in surface morphology, geology, and climate, this variability is expected.

5.3. Contributions of earthquake-triggered landslides to erosion

We next determine the rate at which earthquakes contribute to erosion. Our approach is similar to that used by Keefer [4]. However, he used actual earthquakes in a region, whereas we will use the statistical distribution of earthquakes occurring in a specified region. This will allow us to obtain an analytic expression for the total landslide volume per unit time triggered by earthquakes in seismogenic regions.

The rate at which earthquakes occur in a region generally satisfies the Gutenberg–Richter frequency–magnitude relation [21]

$$\log \dot{N}_{CE} = -bM + \log \dot{a} \qquad (20)$$

where $\dot{N}_{CE}$ is the cumulative number of earthquakes with a moment magnitude greater than or equal to M in a specified area and time. The constant b or 'b value' varies from region to region but is generally in the

range $0.8 < b < 1.2$ [22]. The constant $\dot{a}$ is a measure of the regional level of seismicity and the size of the area being considered. In deriving the erosion rate associated with seismically triggered landslides, we will assume the validity of Eq. (20) for all earthquakes in a region [23]. There are upper and lower magnitude limits to the validity of Eq. (20), and whether the largest characteristic earthquakes in a region fall on the extrapolation of the regional Gutenberg–Richter scaling is a subject of controversy. Some authors (e.g., [24]) argue that the large earthquakes occur more often than would be predicted by an extrapolation. In this case, the rates of erosion due to seismically induced landslides would be even higher than the ones we derive below.

We next combine the rate of occurrence of earthquakes $\dot{N}_{CE}$ given by Eq. (20) with the relationship between the earthquake moment magnitude and the total volume of all associated landslides, given by Eq. (14), to get the rate of earthquake-induced landsliding. The volume rate $\dot{V}_L$ at which landslide material is generated by earthquakes is obtained by integrating the total volume V_{LT} of landslide material generated by each individual earthquake of moment magnitude M. This integral is carried out over the magnitude range $M_{min} \leq M \leq M_{max}$, giving

$$\dot{V}_L = -\int_{M_{min}}^{M_{max}} V_{LT}[M] \mathrm{d}\dot{N}_{CE}[M] \qquad (21)$$

Rewriting Eq. (20) as

$$\dot{N}_{CE} = \dot{a}10^{-bM} \tag{22}$$

and taking its derivative with respect to magnitude M gives

$$d\dot{N}_{CE} = -b\dot{a}(\ln 10)10^{-bM}dM \tag{23}$$

with ln10, the natural log of 10. We rewrite Eq. (14) in the form

$$V_{LT} = 10^{-11.26\pm0.52}10^{1.42M} \tag{24}$$

with V_{LT} in km^3. Substitution of Eqs. (23) and (24) into Eq. (21) gives

$$\dot{V}_L = 10^{-11.26\pm0.52}(\ln 10)b\dot{a}\int_{M_{min}}^{M_{max}}10^{(1.42-b)M}dM \tag{25}$$

with $\dot{a}$ in year^{-1} and $\dot{V}_L$ in km^3 year^{-1}. Since $0.8 < b < 1.2$ [22], this integral diverges for large earthquakes and converges for small earthquakes, thus, the lower limit M_{min} can be taken to be $-\infty$. After integration, we have

$$\dot{V}_L = \frac{10^{-11.26\pm0.52}b\dot{a}}{1.42-b}10^{(1.42-b)M_{max}} \tag{26}$$

again with $\dot{a}$ in year^{-1} and $\dot{V}_L$ in km^3 year^{-1}. The volume rate of landslide-generated material is strongly dependent on the moment magnitude of the largest earthquake in a region.

As a specific application of these results, we will consider southern California. The Gutenberg–Richter parameters for southern California [25] are $b=0.923$ and $\dot{a}=1.4\times10^5$ year^{-1}. This seismicity occurs over an area of about 240,000 km^2. The equivalent $\dot{a}$ for a 1 km^2 area is 0.58 year^{-1}. Based on the paleoseismic estimate of the 1857 great southern California earthquake [26], we take $M_{max}=8.05$. Substitution of $\dot{a}=1.4\times10^5$ year^{-1}, $b=0.923$, and $M_{max}=8.05$ into Eq. (26) gives $\dot{V}_L=0.0043$–0.047 km^3 year^{-1}. Averaging over the entire 240,000 km^2 seismically active region, the mean erosion rate for southern California due to seismically induced landslides is $\dot{h}=0.02$–0.2 mm year^{-1}.

Keefer [4] has also estimated the erosion rate in southern California due to seismically induced land-slides. He used his empirical relationship between landslide volumes and earthquake moments magnitudes to determine the total landslide volume triggered by historic earthquakes. He averaged the total land-slide volume over an area of 70,000 km^2 and obtained erosion rates over the range $\dot{h}=0.04$–0.08 mm year^{-1}. His values fall within our estimates.

5.4. Landslides generated by aftershocks

Aftershocks can also generate landslides. We now quantify the relative contribution of aftershocks to erosion due to the associated landslides. Båth's Law [27] states that the largest aftershock will have a magnitude about 1.2 units less than the mainshock. Comparing the results using $(M-1.2)$ in place of M in Eqs. (14) and (16), we find that the largest aftershock contributes just 3.0% of the total area A_{LT} and 2.0% of the total volume V_{LT} of landslides triggered by the mainshock. Aftershocks generally follow the Gutenberg–Richter scaling. Using the approach outlined in Eqs. (24)–(26), and taking $b=0.9$, we find that the contribution of *all* aftershocks is about 17% of the total area A_{LT} and 8.0% of the total volume V_{LT} of landslides triggered by the mainshock. Therefore, aftershocks contribute relatively little to the total volume of associated landslides and erosion.

5.5. Global seismically induced erosion

We next relate the erosion rate $\dot{h}$ due to earthquake-induced landslides to the intensity of seismicity in 1° long.×1° lat. regions on a global scale. Kossobokov et al. [28] introduced the concept of a seismic-intensity factor I_M, the number of earthquakes per year with magnitudes greater than or equal to M occurring in 1°×1° areas and normalized by the cosine of the latitude. The normalization is required because the areas of the 1°×1° boxes change with changing latitude. These authors produced a global map of I_4 (number of magnitude $M\geq4$ earthquakes) using the NEIC Hypocenter Data Base [29] for the period 1964–1995. The magnitude 4 cutoff was taken to assure a relatively complete catalog of seismicity in seismically active areas. Magnitudes were systematically reported in the NEIC Hypocenter Data Base [29] as moments from 1976–1995, whereas before 1976, a variety of magnitudes were used. For very active parts of the 'ring

of fire' around the Pacific, I_4 was found to be in the range 5–15 earthquakes year^{-1} in the normalized $1° \times 1°$ areas. For California, Guatemala, New Zealand, and southeastern Europe (Italy, Greece, and Turkey), and typical of areas adjacent to plate boundary strike-slip faults, I_4 was found to be in the range 1–5 earthquakes year^{-1} in the normalized $1° \times 1°$ areas.

To associate the erosion rate $\dot{h}$ to the seismic intensity factor I_4, we relate I_4 to the Gutenberg–Richter parameter $\dot{a}$ using Eq. (22). Taking an average value of $b=0.9$, we obtain

$$\dot{a} = I_4 10^{3.6} \tag{27}$$

For $I_4=1$ earthquake year^{-1}, we find $\dot{a} \cong 4.0 \times 10^3$ year^{-1} in each (normalized) $1° \times 1°$ box, an area of about 111×111 km^2 (equivalent area at the equator). Therefore, for a 1 km^2 region, $\dot{a}=0.32$ year^{-1}. This compares with the value $\dot{a}=0.58$ year^{-1} given previously for a 1 km^2 area in southern California.

The volume rate $\dot{V}_L$ at which landslide material is generated by earthquakes with $M \geq 4$ is obtained by the substitution of Eq. (27) and $b=0.9$ into Eq. (26), giving

$$\dot{V}_L = 3.79 \times 10^{-8} I_4 10^{0.52(M_{max} \pm 1)} \tag{28}$$

with $\dot{V}_L$ in km^3 year^{-1}. The erosion rate $\dot{h}$ due to landslides triggered by all earthquakes with $M \geq 4$ is then obtained from Eq. (28) divided by 111×111 km^2, giving

$$\dot{h} = 3.08 \times 10^{-6} I_4 10^{0.52(M_{max} \pm 1)} \tag{29}$$

with $\dot{h}$ in mm year^{-1}.

The dependence of the seismically induced erosion rate $\dot{h}$ on the seismic intensity factor I_4 is given in Fig. 6 for $M_{max}=7$, 8, and 9. Using Eq. (29) for the very active subduction zones of the Pacific 'ring of fire' ($I_4 \approx 5$–15 earthquakes year^{-1} in normalized $1° \times 1°$ areas, $M_{max} \approx 9$), we find predicted rates of seismically induced erosion in the range $\dot{h}=0.2$–7 mm year^{-1}. In contrast, for areas adjacent to plate boundary strike-slip faults ($I_4 \approx 1$–5 earthquakes year^{-1} in normalized $1° \times 1°$ areas, $M_{max} \approx 8$), the predicted rates of seismically induced erosion are in the range $\dot{h}=0.01$–0.7 mm year^{-1}. Again, we emphasize that this approach has many uncertainties.
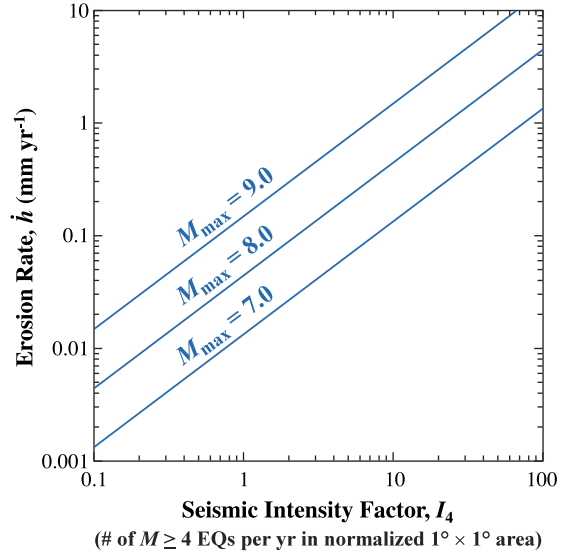

Fig. 6. Dependence of the seismically induced erosion rate $\dot{h}$ on the seismic intensity factor I_4 using Eq. (29) and taking the maximum earthquake $M_{max}=7$, 8, and 9.

However, with the large uncertainties associated with erosion rates, we believe that our estimates, even with their range and errors, are useful.

6. Discussion and conclusions

In this paper, we have utilized a general landslide distribution to relate landslide inventories to erosion rates and provide quantitative estimates of the landslide hazard associated with earthquakes. There are several important implications of the applicability of a general landslide distribution. It provides the basis for defining a landslide-event magnitude scale $m_L=\log N_{LT}$, with N_{LT} being the total number of landslides in the landslide event. The direct determination of the landslide-event magnitude requires that the landslide inventory be complete. However, the general landslide distribution can be used to determine a landslide-event magnitude from a partial inventory, where the inventory is complete only for landslide areas greater than a specified value. It can also be used for historical inventories, which include the sum of landslide events over time. Using the general landslide distribution, the total area and volume of associated landslides in the event or sum of events

over time, as well as the area and volume of the maximum landslides, can be directly related to the landslide-event magnitude m_L.

The general landslide distribution has also been used here to quantify the landslide hazard associated with earthquakes. Keefer [4] proposed an empirical power-law relation between the logarithm of the total volume of landslides generated by an earthquake and the earthquake moment magnitude. Using this correlation and the general landslide distribution, we have obtained analytical relationships between an earthquake's moment magnitude M and the associated landslide-event magnitude m_L, the total number of landslides, the average landslide area and volume, the total landslide area and volume, and the maximum landslide area and volume. We use these relationships to estimate that the minimum earthquake magnitudes that will generate landslides is $M=4.3\pm0.4$, in agreement with observations, and also to estimate upper and lower bounds for landslide statistics triggered by a great earthquake ($M=8$) in southern California.

In the last section of this paper, we have used estimates of total landslide volumes to quantify erosion based on landslide inventories, individual earthquakes, and overall global seismicity. Using estimated recurrence intervals for three landslide events and the time span for two historical inventories, with estimates for areas over which the landslides are concentrated, we have derived associated regional erosion rates, $\dot{h} \approx 0.1$–2.5 mm year^{-1}. Using the Gutenberg–Richter frequency–magnitude relation for earthquakes, we have obtained an analytic expression for the volumetric rate of generation of landslide debris in terms of the intensity of the regional seismicity. Applying this correlation to southern California, we find that the rate of erosion due to earthquake-generated landslides is $\dot{h} \approx 0.02$–0.2 mm year^{-1}. Finally, we have derived a relationship between the intensity of seismicity in $1°\times1°$ areas on a global scale, the moment magnitude of the largest expected earthquake in the region, and associated erosion rates. We find that typical seismically induced erosion rates in very active subduction zones such as Japan and Chile are $\dot{h} \approx 0.2$–7 mm year^{-1}, and adjacent to plate boundary strike-slip fault zones, such as the San Andreas Fault in California and the North Anatolian Fault in Turkey, are $\dot{h} \approx 0.01$–0.7 mm year^{-1}. It is likely that bedrock landslides and massive rock falls are dominant contributors to the long-term erosion in seismically active tectonic zones.

In closing, we briefly discuss landslides and their relationship to metastable clusters. Landslides are usually the results of slope instabilities in tectonically active areas. Compressional and extensional tectonics generates topography due to displacement on faults. These displacements also generate the ground shaking responsible for the landslides. Hillslopes become metastable regions susceptible to landsliding. A weak trigger will result in landslides in a few of these metastable regions. A strong trigger will result in a large number of landslides. As a mountainous region evolves tectonically, metastable regions grow and coalesce. Turcotte et al. [30] showed that this static growth of metastable regions is a self-similar process that yields a power-law frequency–size distribution. The concept of metastable regions that satisfy the general probability distribution given in Eq. (3) potentially explains why this distribution might be valid for landslide events of different sizes. The magnitude of the earthquake trigger determines the magnitude of the landslide event. The frequency–area distribution of landslides is determined by the frequency–area distribution of metastable regions, independent of the magnitude of the trigger.

Appendix A. Variables used in text

Variable	Description	Equation introduced
$\delta N_L / \delta A_L$	δN_L is the number of landslides with areas between A_L and $A_L + \delta A_L$	1
ε	Coefficient in $V_L = \varepsilon A_L^{1.50}$	10
$\Gamma(\xi)$	Gamma function, $\Gamma(\xi) = \int_0^\infty y^{\xi-1} \exp(-y) dy, \xi > 0$	3
ρ	Parameter primarily controlling power-law decay for medium and large values in three-parameter inverse-gamma probability distribution	3
τ_L	Recurrence interval in time of a given landslide event	19
a	Parameter primarily controlling location of maximum probability in three-parameter inverse-gamma probability distribution	3
$\dot{a}$	Constant in the Gutenberg–Richter frequency–magnitude relation	20
b	Constant in the Gutenberg–Richter frequency–magnitude relation	20
A_L	Area of landslide	1
$\bar{A}_L$	Average area of landslides associated with a landslide event	4
A_{Lmax}	Maximum landslide area associated with a landslide event	8
A_{LT}	Total area of landslides associated with a landslide event	6
A_R	Regional area over which landslides are concentrated	19
$f(A_L)$	Frequency density of landslide areas: the number of landslides δN_L with areas between A_L and $A_L + \delta A_L$, divided by the width of that bin, δA_L	13
$\dot{h}$	Erosion rate	19
I_4	Number of earthquakes per year with $M \geq 4$, occurring in $1° \text{ lat.} \times 1° \text{ long.}$ areas, normalized by cosine of lat.	27
M	Earthquake magnitude	14
m_b, M_L, M_s	Earthquake magnitudes: body-wave, local, and surface-wave	(no equation)
m_L	Magnitude of a landslide event, with $m_L = \log N_{LT}$	11
M_{max}, M_{min}	Maximum and minimum earthquake moment magnitudes in specified area and time	21
$\dot{N}_{CE}$	The cumulative number of earthquakes with magnitude greater than or equal to M in a specified area and time	20
N_{LT}	Total number of landslides in an inventory	1
$p(A_L)$	Probability density: the frequency density, $f(A_L)$, divided by the total number of landslides, N_{LT}, in a substantially complete landslide inventory	1
s	Parameter primarily controlling exponential rollover for small values in three-parameter inverse-gamma probability distribution	3
V_L	Volume of landslide	10
$\bar{V}_L$	Average volume of landslides associated with a landslide event	5
$\dot{V}_L$	Volume rate at which landslide material is generated by earthquakes	21
V_{Lmax}	Maximum landslide volume associated with a landslide event	9
V_{LT}	Total volume of landslides associated with a landslide event	7

References

[1] B.D. Malamud, D.L. Turcotte, F. Guzzetti, P. Reichenbach, Landslide inventories and their statistical properties, Earth Surf. Process. Landf. 29 (2004) 687–711.

[2] V. Kobayashi, Causes of fatalities in recent earthquakes in Japan, J. Dis. Sci. 3 (1981) 15–22.

[3] D.K. Keefer, Landslides caused by earthquakes, Geol. Soc. Am. Bull. 95 (1984) 406–421.

[4] D.K. Keefer, The importance of earthquake-induced landslides to long-term slope erosion and slope-failure hazards in seismically active regions, Geomorphology 10 (1994) 265–284.

[5] D.K. Keefer, Investigating landslides caused by earthquakes—a historical review, Surv. Geophys. 23 (2002) 473–510.

[6] E.L. Harp, R.L. Jibson, Inventory of landslides triggered by the 1994 Northridge, California earthquake, Open-File Rep. (U. S. Geol. Surv.) 95–213 (1995).

[7] E.L. Harp, R.L. Jibson, Landslides triggered by the 1994 Northridge, California earthquake, Bull. Seismol. Soc. Am. 86 (1996) S319–S332.

[8] M. Cardinali, F. Ardizzone, M. Galli, F. Guzzetti, P. Reichenbach, Landslides triggered by rapid snow melting: the December 1996–January 1997 event in Central Italy, in: P.P. Claps, F. Siccardi (Eds.), Proceedings 1st Plinius

Conference on Mediterranean Storms, Maratea, Italy, 14–16 October 1999, Bios., Cosenza, 2000, pp. 439–448.

[9] F. Guzzetti, B.D. Malamud, D.L. Turcotte, P. Reichenbach, Power-law correlations of landslide areas in central Italy, Earth Planet. Sci. Lett. 195 (2002) 169–183.

[10] R.C. Bucknam, J.A. Coe, M.M. Chavarría, J.W. Godt, A.C. Tarr, L.-A. Bradley, S. Rafferty, D. Hancock, R.L. Dart, M.L. Johnson, Landslides triggered by Hurricane Mitch in Guatemala—inventory and discussion, Open-File Rep. (U. S. Geol. Surv.) 01–443 2001, (38 pp.).

[11] N.L. Johnson, S. Kotz, Continuous Univariate Distribution, John Wiley, New York, 1970, 300 pp.

[12] M. Evans, N. Hastings, J.B. Peacock, Statistical Distributions, 3rd ed., John Wiley, New York, 2000, 248 pp.

[13] N. Hovius, C.P. Stark, P.A. Allen, Sediment flux from a mountain belt derived by landslide mapping, Geology 25 (1997) 231–234.

[14] C.E. Rodríguez, J.J. Bommer, R.J. Chandler, Earthquake-induced landslides: 1980–1997, Soil Dyn. Earthqu. Eng. 18 (1999) 325–346.

[15] F. Guzzetti, P. Reichenbach, M. Cardinali, F. Ardizzone, M. Galli, Impact of landslides in the Umbria Region, Central Italy, Nat. Hazards Earth Syst. Sci. 3 (2003) 469–486.

[16] H. Ohmori, T. Sugai, Toward geomorphometric models for estimating landslide dynamics and forecasting landslide occurrence in Japanese mountains, Z. Geomorphol., Suppl. Bd 101 (1995) 149–164.

[17] J.J. Bommer, C.E. Rodríguez, Earthquake-induced landslides in Central America, Eng. Geol. 63 (2002) 189–220.

[18] T. Lay, T.C. Wallace, Modern Global Seismology, Academic Press, San Diego, CA, 1995, 517 pp.

[19] R.W. Jibson, Use of landslides for paleoseismic analysis, Eng. Geol. 43 (1996) 291–323.

[20] D.W. Burbank, Rates of erosion and their implications for exhumation, Mineral. Mag. 66 (1) (2002) 25–52.

[21] B. Gutenberg, C.F. Richter, Seismicity of The Earth and Associated Phenomenon, 2nd ed., Princeton University Press, Princeton, NJ, 1954, 310 pp.

[22] C. Frohlich, S.D. Davis, Teleseismic b values; or, much ado about 1.0, J. Geophys. Res. 98 (1993) 631–644.

[23] D.L. Turcotte, B.D. Malamud, Earthquakes as a complex system, in: P. Jennings, H. Kanamori, W. Lee (Eds.), IASPEI, International Handbook of Earthquake and Engineering Seismology, Academic Press, San Francisco, CA, 2002, pp. 209–227.

[24] C.H. Scholz, Size distributions for large and small earthquakes, Bull. Seismol. Soc. Am. 87 (1997) 1074–1077.

[25] D.L. Turcotte, Fractals and Chaos in Geology and Geophysics, 2nd ed., Cambridge University Press, Cambridge, 1997, 398 pp.

[26] K.E. Sieh, Slip along the San Andreas fault associated with the great 1857 earthquake, Bull. Seismol. Soc. Am. 68 (1978) 1421–1448.

[27] M. Båth, Lateral inhomogeneities in the upper mantle, Tectonophysics 2 (1965) 483–514.

[28] V.G. Kossobokov, V.I. Keilis-Borok, D.L. Turcotte, B.D. Malamud, Implications of a statistical physics approach for earthquake hazard assessment and forecasting, Pure Appl. Geophys. 157 (11–12) (2000) 2323–2349.

[29] GHDB, Global Hypocenter Data Base, [CD ROM] NEIC/ USGS, Denver, CO, 1989, and its updates through 1997.

[30] D.L. Turcotte, B.D. Malamud, G. Morein, W.I. Newman, An inverse-cascade model for self-organized critical behavior, Physica A 268 (1999) 629–643.